ELSEVIER

International Journal of Mass Spectrometry 219 (2002) 717–727

International Journal of Mass Spectrometry

www.elsevier.com/locate/ijms

The resonance laser ablation Fourier-transform ion cyclotron resonance mass spectrometry (RLA-FTICRMS) a new coupling for material science

Frédéric Aubriet*, Lionel Vernex-Loset, Benoît Maunit, Gabriel Krier, Jean-François Muller

Laboratoire de Spectrometrie de Masse et de Chimie Laser, IPEM, Université de Metz—1, Boulevard Arago, 57078 Metz Cedex 03, France

Received 26 March 2002; accepted 29 April 2002

Dedicated to Dr. Yannik Hoppilliard on the occasion of her 60th birthday.

Abstract

The development of a new device, which associated resonant ionization and Fourier-transform ion cyclotron resonance mass spectrometry by coupling a tunable laser with the laser microprobe Fourier-transform ion cyclotron resonance mass spectrometry (FTICRMS) developed at the University of Metz, allowed us to carry out the first resonance laser ablation Fourier-transform ion cyclotron resonance mass spectrometry (RLA-FTICRMS) experiments. RLA-FTICRM ensures, due to the involved processes, an increase in the selectivity and sensitivity of the ionization and a high mass resolution by the use of a FTICR mass spectrometer. These potentialities lead us to consider this new technique as a tool of choice for the analysis of inorganic traces by resonant laser ablation/ionization mass spectrometry (RLA-MS). The first experiments reported in this study ensures a 2–7 benefit in selectivity, according to the studied matrix and a limit of detection lower than 1 ppm for chromium. Finally, the influence of the power density on the involved processes was highlighted and allowed us to determine that the resonant processes are most effective for power density lower than 5×10^8 W/cm^2. (Int J Mass Spectrom 219 (2002) 717–727)

Keywords: Resonant laser ablation; Trace analysis; Mass spectrometry; Ionization; Chromium

1. Introduction

Resonant ionization mass spectrometry (RIMS) is a technique that takes advantage of resonant ionization spectrometry (RIS) and mass spectrometry (MS). In this particular type of ionization, ion formation takes place via one or more intermediate states. In the simplest case (two-photon process), a photon is absorbed by an atom in the gas phase, which allows the transition from the fundamental level to a 'long-lived' excited energy level to be achieved. This level has typically a lifetime of several tens of nanoseconds. From this excited state, the absorption of a second photon leads to ionization. In resonant ionization, the photons are produced by tunable laser(s), which are adjusted to intense absorbing line(s) of the studied atom [1]. A resonance setup involves typically several

* Corresponding author.
E-mail: aubriet@lsmcl.sciences.univ-metz.fr, jfmuller@lsmcl.sciences.univ-metz.fr

1387-3806/02/$ – see front matter
PII S1387-3806(02)00750-9

tunable lasers, which allow the excitation and the ionization of the atoms in the gas phase to be achieved according to reversible electronic transitions from the atom studied via one of the five basic diagrams proposed by Hurst et al. [1].

In RIMS experiments, atom transfer from the solid to the gas phase can be performed by several methods. It consist mainly in sample sublimation, laser ablation or ion sputtering. The thermal methods are the least common [2–5], the methods by ion sputtering (generally with Ar^+ ions) [6–13] or by laser ablation [8,14–18] (typically in the ultraviolet regime) are the most used methods because of their versatility. The analytical use of RIMS has been recognized for a long time for its selectivity and sensitivity, but several original works have recently been published which show the potential of this method for the semi-conductor science [16], for the detection of plutonium ultra-traces in environmental samples after the Chernobyl accident [19–21], or to determine isotopic ratios [2,9,20,22] or the first ionization energy of actinides [5].

However, the use of several tunable lasers on one hand and of a vaporization sample device on the other hand, complicates the routinely use of this technique. In contrast, resonant laser ablation/ionization mass spectrometry (RLA-MS) is easier to use. This technique was developed in our laboratory since 1984 [23,24]. It ensures the selective ionization of a chemical element by multiphoton processes (generally two-photon ones) by the use of only one laser shot on a solid sample (i.e., both steps of vaporization/ablation and resonant ionization are carried out by photons from the same laser pulse).

Previous studies carried out by RLA involved the coupling of a dye laser with a time-of-flight mass spectrometer (ToF-MS). They are conducted to analyze metallic traces in various matrices or to select a metal ion for ion–molecule reactions [25]. Specifically, the resonant ablation/ionization of an alloy containing chromium, iron, copper and nickel allowed a metal to be selected for reaction with acetone. That kind of experiments is impossible in non-resonant ablation ionization mode without including selective ion ejection with an FTICR mass spectrometer [26]. The work performed by RLA-ToF-MS in our laboratory [24,27–30] enabled us to obtain a significant know-how, especially for the speciation of metal oxides [28,30]. RLA-MS has also been used by Gibson in the study of lanthanide trivalent oxides, lanthanide oxalates [31] and actinide dioxide [32].

However, the obtained increase of selectivity with RLA-MS is definitely lower than that obtained by RIMS and isobaric interferences may occur in RLA-MS experiments [10]. In this context, ion cyclotron resonance mass spectrometry (ICR-MS) constitutes a method of choice.

Therefore, we investigated the capabilities of a new coupling between a tunable dye laser and a FTICR mass spectrometer for RLA-FTICRMS experiments. The ionization mode selectivity, the sensitivity and the high mass resolution of an FTICRMS instrument should make this coupling a powerful tool in the analysis of traces by mass spectrometry. We will describe in this paper, the experimental device, the performances of the used tunable dye laser, the first obtained results and the power density influence on the processes involved in RLA-FTICRMS experiments.

2. Experimental

Fig. 1 presents our new experimental device. It consists of four distinct elements: (i) a Nd:YAG pumping laser at 532 nm, (ii) a tunable dye laser, (iii) an optical bench, and (iv) a laser microprobe Fourier-transform ion cyclotron resonance mass spectrometer. The latter two elements were designed and built at the laboratory at the beginning of the 1990s.

2.1. The microprobe FTICRMS and the optical bench

These analyses were performed using a laser microprobe FTICR mass spectrometer that has been described in detail elsewhere [33,34]. This instrument is a modified differentially pumped, dual-cell Nicolet Instrument FTMS 2000 (Finnigan FT/MS, now ThermoQuest, Madison, WI, USA) operated with a

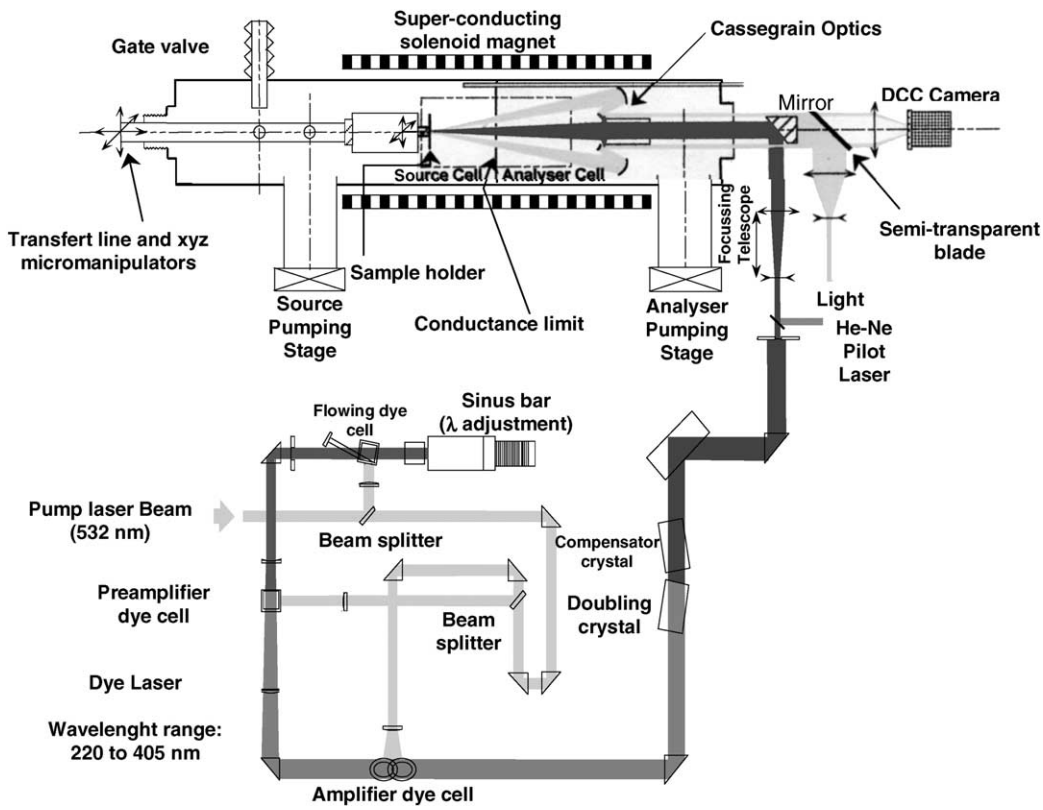

Fig. 1. Coupling of the tunable dye laser TDL 90 with a FTICR mass spectrometer.

3.04 Torr magnetic field and coupled to a reflection laser interface. The viewing system, using an inverted Cassegrain optics, allows the sample to be visualized with 300-fold magnification. A sample probe fitted with motorized micromanipulators into the three spatial directions permits attainment of a spatial accuracy of less than 10 μm. The diameter of the laser beam on the sample (placed inside the source cell) can be adjusted by means of the internal lenses and an external adjustable telescope from 5 μm to several hundred μm, which corresponds to a power density ranging from 10^6 to 10^{10} W/cm^2. The experimental sequence used for these analyses is as described: ions are formed by laser ablation in the source cell (residual pressure less than 10^{-6} Pa). During the ionization event, the conductance limit plate between the two cells and the source trap plate are kept at a trapping potential of typically 1 V (−1 V in negative detection mode, respectively) or a lower potential in some cases (down to 0.25 V). A variable delay period follows, during which ion–molecule reactions can occur. Ions are then excited by a frequency excitation chirp and the resulting image current is detected, amplified, digitized, apodized (Blackman-Harris, three-terms) and Fourier-transformed to produce a mass spectrum. Each FTICR mass spectrum resulted generally, from an average of 100 laser shots fired on consecutive spots.

2.2. The pumping laser and the tunable dye laser

The pumping of the dye laser is ensured by a Brilliant B laser of Quantel (Les Ulis, France). This Nd:YAG laser delivers a nominal energy of 400 mJ at the wavelength of 532 nm. Under our standard

Table 1
Laser beam energy at different wavelengths obtained according to the mode and the used dye

Dye	Rhodamine 590	Rhodamine 610 + Rhodamine 640	LDS 698
Mode used			
Direct	560 nm: 105 mJ	584 nm: 90 mJ	698 nm: 60 mJ
Doubled	280 nm: 22 mJ	295 nm: 22 mJ	357.87 nm: 12 mJ
Mixed	221.7 nm: 4 mJ	–	–

operating conditions the analytical FTICRMS sequence time is equal to 1 s, that is the reason why the pumping laser is optimized at 1 Hz. The dye laser is a TDL 90 laser built by Quantel (Les Ulis, France). The dyes: Rhodamine 590, 610 and 640; LDS 698 and 740 (Exciton distributed by Opticas, France) are used to obtain, in direct mode, wavelengths between 550 and 820 nm. The frequency doubling crystal allows wavelengths ranging from 275 to 400 nm to be obtained. Finally, the additional use of a mixer crystal ensures, according to the used dye, to obtain wavelengths, between 218.5 and 278 nm. Chromium and nickel RLA-MS studies were performed with LDS 698 dye pumped at the 532 nm wavelength which allows us, in doubling mode, to reach the chromium and nickel resonance lines at 357.87 and 352.45 nm, respectively. The pulse duration of the tunable laser is 4.3 ns. A prism allows the emergent laser beam to be directed towards the optical bench of the FTICRMS instrument. Finally, a mirror directs the ionizing laser beam inside the mass spectrometer chamber. The use of a lens with a short focal distance ensures to obtain power densities greater than 10^{10} W/cm^2.

2.3. TDL 90 dye laser performances

In order to determine as well as possible the potentially of this new device, several tests were implemented. Several dyes were in particular studied in order to determine for each one the obtained energy in direct and doubled modes. Some tests in mixed mode were also carried out. The three studied dyes are: Rhodamine 590, a mixture of Rhodamine 610 and 640 dissolved in ethanol and LDS 698 dissolved in methanol. The results of the various tests are reported in Table 1. The optical devices absorb nearly 90% of the laser beam energy. Nevertheless, the laser fluence typically required in our experiments, is only about some tenth of millijoules, which is in the laser energy range obtained using the tunable dye laser TDL 90.

3. Results

3.1. Benefit in sensitivity and selectivity

Three kinds of samples were analyzed: the chromium–nickel NIMONIC alloy; a glass and finally a cement. These three samples contain 20, 2 and 0.02 wt.% of chromium, respectively. Experiments were carried out with the chromium resonance line at 357.87 nm and in non-resonant mode at 355 nm.

Fig. 2 reports the results obtained in the study of an alloy including nickel (76%), chromium (20%) and titanium (4%). Experiments were undertaken with three different wavelengths: 355, 357.87 and 352.45 nm. The first wavelength corresponds to a standard ablation wavelength. The two following ones are resonance lines for chromium and nickel, respectively. The chromium ionization at 357.87 nm corresponds to a two-photon process: the first photon allows the transition from the fundamental $^7S_3$ to the $^7P_4$ excited state, the second one ensures ionization (Fig. 3a). At 352.45 nm, the nickel resonant ionization (Fig. 3b), involves also a two-photon process. The absorption of the first photon allows the transition from the slightly excited $^3D_3$ level towards the $^3P_2$ one to be achieved. The absorption of a second photon allows to reach the ionization threshold. The intensities of the resonant lines used in this study are 2400 and 750 for chromium and nickel, respectively [35]. To evaluate the selectivity benefit obtained in RLA-FTICRMS

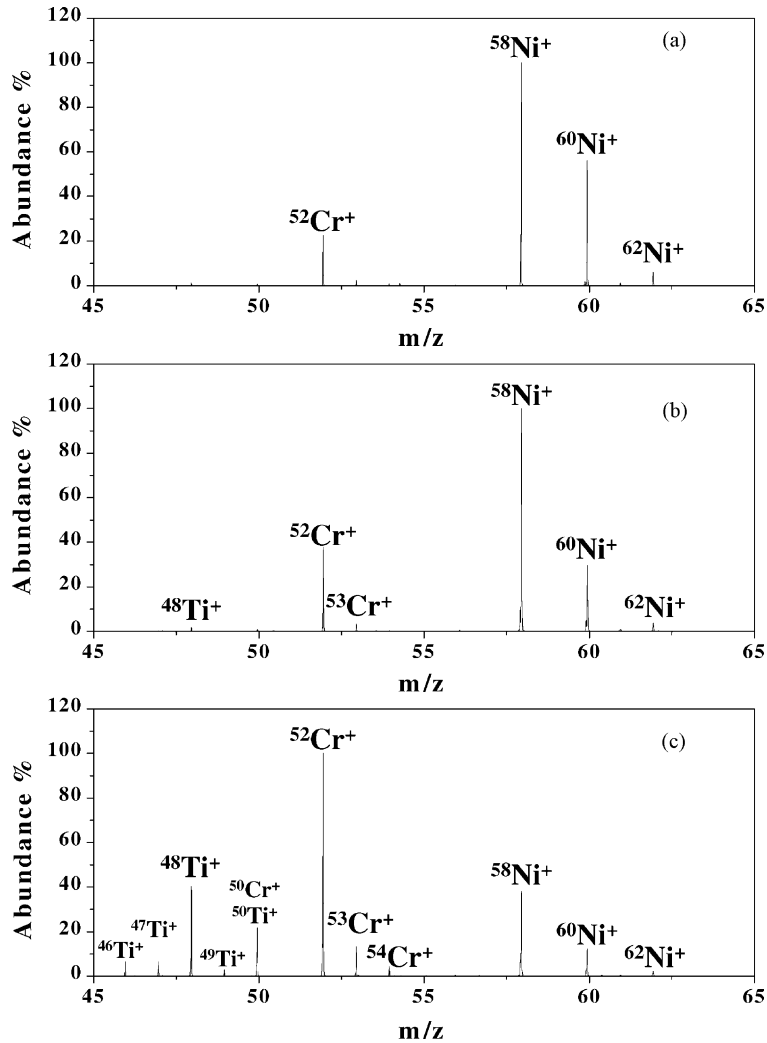

Fig. 2. Chromium–nickel alloy FTICRMS analysis in resonance laser ablation/ionization mode of (a) nickel and (c) chromium at 352.45 and 357.87 nm, respectively, and (b) in standard ionization mode at 355 nm.

experiments, the R ratio was calculated:

$$R = \frac{\sum_i I_{i\,\mathrm{Cr}^+}}{\sum_j I_{j\,\mathrm{Ni}^+}}$$

it corresponds to the sum of the chromium isotope intensities except for $^{50}Cr^+$, due to interference with $^{50}Ti^+$, on the sum of all nickel isotopes ($^{58}Ni^+$, $^{60}Ni^+$, $^{61}Ni^+$, $^{62}Ni^+$ and $^{64}Ni^+$).

According to the high mass resolution of FTICR mass spectrometer, $^{50}Ti^+$ and $^{50}Cr^+$ ions could be easily separated. Fig. 4 reported a high mass resolution spectra obtained in the study in the mass range between m/z 47.25 and 52.25. The mass resolution and the accurate mass measurement obtained in this experiment (see Table 2) allow us to distinguish and to identify without ambiguity titanium and chromium isotope. The results obtained with $^{49}Ti^+$ and $^{51}V^+$ (small amounts of sodium metavanadate were deposited at the surface of the sample) confirmed these results. The peaks observed around $^{48}Ti^+$ and $^{52}Cr^+$

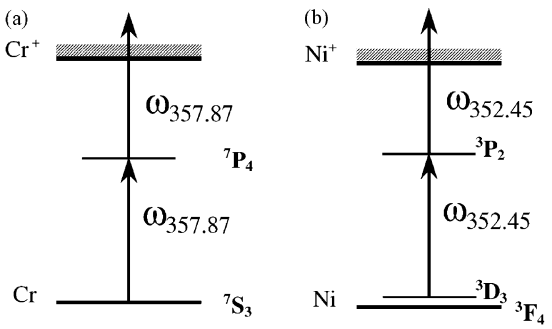

Fig. 3. Simplified energy level diagrams for (a) chromium and (b) nickel ionization at 357.8 and 352.45 nm, respectively.

Table 2
Mass measurement and resolving power obtained in the study of NEMONIC alloy in high mass resolution mode

Ion	*m/z*		Resolving power
	Theoretical	Experimental	
$^{48}Ti^+$	47.94740	*Reference ion*	130914
$^{49}Ti^+$	48.94733	48.94731	99585
$^{50}Ti^+$	49.94424	49.94425	108216
$^{50}Cr^+$	49.94550	49.94546	86744
$^{51}V^+$	50.94341	50.94342	90693
$^{52}Cr^+$	51.93996	*Reference ion*	75046

ions came from the excitation of the ions during the FTICRMS sequence which began and ended at frequencies close to cyclotronic frequency of $^{48}Ti^+$ and $^{52}Cr^+$ ions. The increase of the mass range to observe all of the titanium, chromium and nickel isotopes led to a decrease of resolving power. In these conditions, it was not possible to distinguish between $^{50}Ti^+$ and $^{50}Cr^+$ ions. That is the reason why we preferred to not considered signal at *m/z* 50 for the quantification of RLA influence in the study of the NEMONIC alloy.

It may be surprising to observe titanium ablation/ionization increase at 357.87 nm. This behavior was previously observed by Gibson [36] when $BaTiO_3$, $Ba_2Lu_4Ti_xO$ and BaF_2 compounds were studied by RLA-ToF-MS with a resonant wavelength of barium. This author suggested that important yield of Ba^{*+} species were also produced during RLA processes. These latter excited ions led to collisional energy transfer to other ablated elements, especially titanium gaseous atoms. Similar processes, involving Cr^{*+} excited ions may be involved in the increase of Ti^+ ion at 357.87 nm. The higher ionization energy of nickel seems to limit these processes when resonant laser ablation of nickel was performed.

The *R* ratio is equal to 0.13 ± 0.02; 0.31 ± 0.06 and 2.20 ± 0.36 at 352.45, 355 and 357.87 nm, respectively. These results show a gain by a factor of about 2.5 when the resonance line of nickel is used and of almost 7 for chromium.

The second sample is a doped glass prepared by mixing 1 mol of silica and 1 mol of PbO lead oxide. Additionally, 2 wt.% of chromium, cobalt and tin and four rare earth compounds (neodymium 1%, samarium 1%, eurpium 1% and gadolinium 1%) have been also added in oxide form. Finally, potash is employed as a melting assistant [34]. Owing to the very strong abundance of lead and the possibility of important isobaric interference between chromium ions and Pb^+

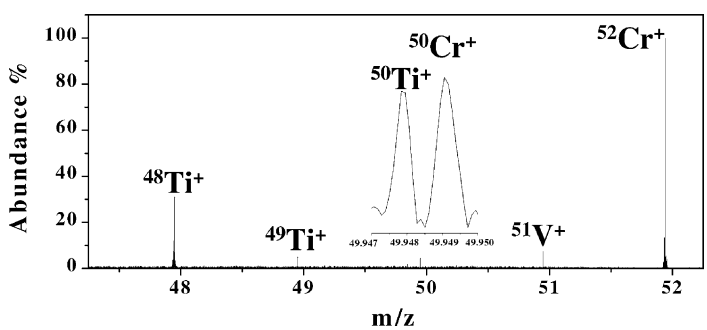

Fig. 4. High mass resolution spectra of NEMONIC alloy in the mass range between *m/z* 47.25 and 52.75.

Table 3
Isotopic ion distribution observed in resonant and non-resonant laser ablation in the study of a doped glass

Ion	Theoretical	355 nm	357.89 nm
$^{50}Cr^+$	4.34	5.02 ± 0.22	4.12 ± 0.32
$^{52}Cr^+$	83.79	81.49 ± 0.58	83.01 ± 1.59
$^{53}Cr^+$	9.50	10.81 ± 0.42	10.05 ± 1.09
$^{54}Cr^+$	2.36	2.68 ± 0.58	2.82 ± 0.60

ion fourth harmonic frequencies, which appear at *m*/*z* 51, 51.5, 51.75 and 52, Pb^+ ions have been partially ejected. Due to this treatment, the Pb^+ ion intensity could not be taken as a reference. That is the reason why the Cr^+ intensity was only compared to the Co^+, Sn^+ and K^+ ion intensities. For example, the Cr^+/K^+ ion intensity ratio at a power density of $\sim 10^8$ W/cm^2 was found to be equal to 0.08 ± 0.01 and 0.64 ± 0.06 at 355 and 357.89 nm, respectively. Moreover, the isotope ratios obtained in our experiments are close to theoretical ones, especially for chromium at 357.87 nm (Table 3).

Finally, the study of cement containing only 200 ppm of chromium has been undertaken. Cement includes alkaline, alkaline-earth, silicon, aluminum and iron oxides. The comparison of the ion intensities at *m*/*z* 52, 39 and 40 relative to $^{52}Cr^+$, $^{39}K^+$ and $^{40}Ca^+$ ions, respectively, shows that the $^{52}Cr^+$ signal increase at 357.87 nm is equal to a factor 3 compared to non-resonant experiments (see Fig. 5). The reproducibility was in this case ~10%.

The study of these three compounds highlights the selectivity of the resonant laser ablation/ionization in various matrices (metallic, vitreous and cement). The examination of samples with decreasing chromium amounts indicates the important sensitivity of RLA-MS when this technique is coupled with the FTICRMS instrument. Contents of about 200 ppm in chromium may be detected in the cement matrix. The detection of the $^{50}Cr^+$ ion, the intensity of which represents 1/20 of that of $^{52}Cr^+$, enables us to consider that the chromium detection limit (DL) in cement matrix is lower than 10 ppm when RLA-FTICRMS is used. A 1 ppm DL (signal-to-noise ratio of 3) may be evaluated for chromium in these experiments. It was

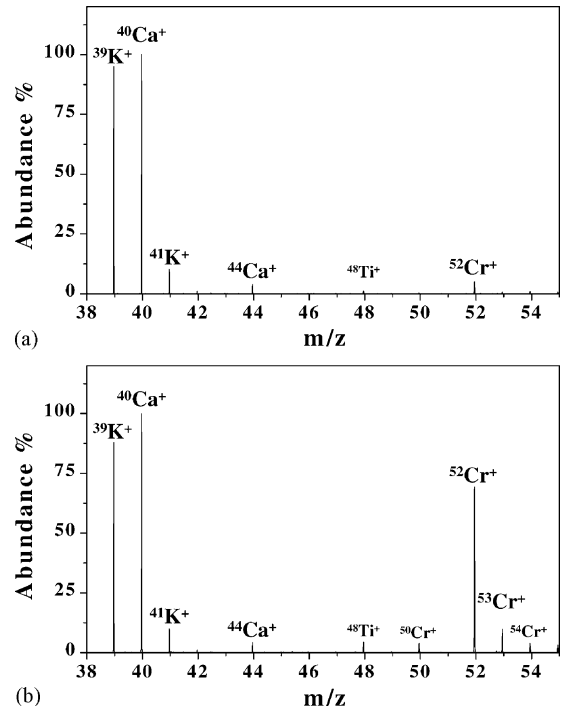

Fig. 5. FTICRMS analysis of a cement containing 200 ppm of chromium (a) in non-resonant at 355 nm, and (b) in chromium resonant mode at 357.87 nm.

not possible to test this detection limit with cement including 1 ppm of chromium. Cement is prepared by mixing and heating at high temperatures clay and lime. Consequently, the amounts of trace element could not be controlled. Moreover, the dilution of industrial cement with calcium silicate, calcium aluminate or calcium iron aluminate, which are the mineral phases of cement is not appropriate. In that case, the absorption properties (i.e., the laser/matter behavior) would be significantly modified.

3.2. *Influence of the laser power density (irradiance)*

The investigations were limited to the examination of the doped glass behavior (2% of chromium). The power density was varied from 4.5×10^{10} to 1.1×10^8 W/cm^2. The experiments in resonant and non-resonant laser ablation/ionization reported in

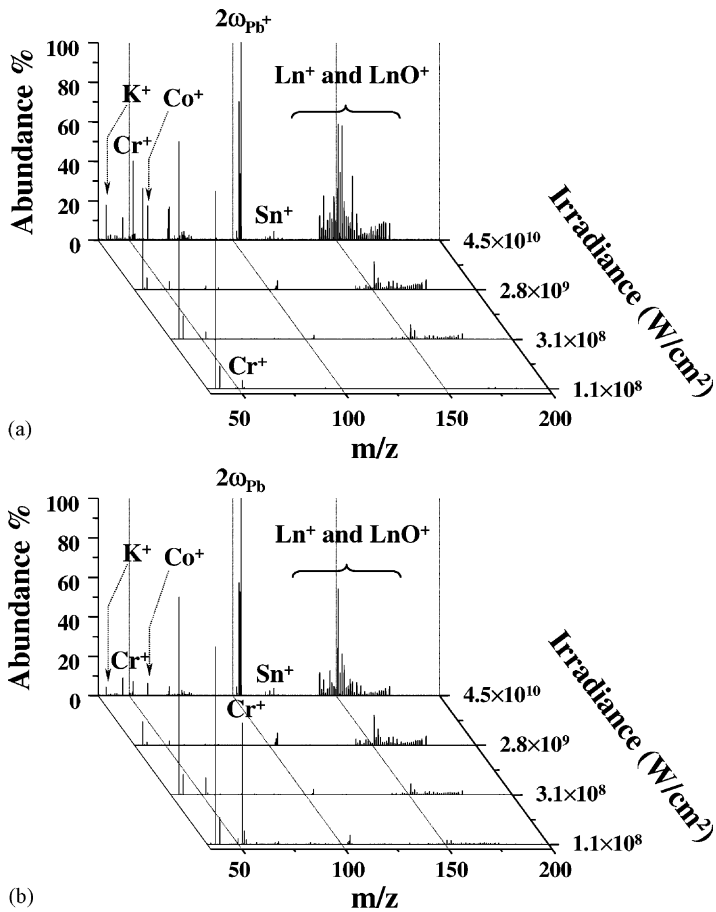

Fig. 6. Development of the doped glass FTICRMS mass spectra as a function of the irradiance at (a) 355 nm and (b) 357.89 nm, respectively. Ln indicates the various lanthanides (neodymium, samarium, europium and gadolinium) and $2\omega_{Pb^+}$ the second harmonic of the Pb^+ ion. Note the difference in Cr^+ ion intensity between (a) 355 nm and (b) 357.89 nm, when low irradiances are used.

Fig. 6, were carried out at 355 and 357.87 nm. It appears clearly that selectivity in the chromium ionization increases when the power density decreases. At high power density, the increase of the chromium ion peak intensity is not significant, whereas it becomes very important when irradiance is lowered to $\sim 10^8$ W/cm^2. This observation is in agreement with the fact that 10–100 times lower irradiances, are required in RLA than in LA experiments. This phenomenon may be explained by considering the involved processes as a function of the power density. At low power density, the plume is cold and transparent and favors multiphoton absorption. At high power density, high temperature, high electronic and ionic densities are reached, which lead to the formation of inverse bremstrahlung [37]. This effect induces photon emission and a high reflectivity of the plume (or plasma). Consequently, the interaction between photons and excited chromium atoms are limited in the gas phase. Finally, the yield of resonant laser ablation/ionization strongly decreases, which causes the loss in sensitivity and selectivity. All experiments reported in this study were carried out with a power density low enough to avoid the formation of an emissive plasma. Moreover, it may be noted that the increase of K^+ ion intensity observed with the

decrease of irradiance was not wavelength depend. The low ionization energy and the low vaporization energy of potassium explained the observed behavior.

3.3. Quantification of resonance effect on the Cr^+ ion signal

Two samples were studied. The first one is a doped glass which contains 2% of chromium and it is representative of purely mineral matrices because it only includes oxides. The second one is organic and corresponds to polystyrene doped with 500 ppm of chromium. The comparison of the results obtained at 355 and 357.87 nm in the doped glass clearly shows that the resonance effect increases in a given power density range. Consequently, the resonant phenomenon importance was studied at a power density of 3×10^8 W/cm^2. To increase the FTICRMS sensitivity, the trapping potential voltage was increased to +1.5 V, which allows to confine more effectively the ions in the FTICR cell. However, raising the trapping potential also increases the harmonic frequency contribution of Pb^+, Nd^+, Sm^+, Eu^+ and Gd^+ ions. The fourth Pb^+ ion harmonics appear in a mass range between $m/z = 51$ and $m/z = 52$, whereas the third lanthanide ion harmonics are observable in the mass range between $m/z = 47.3$ and $m/z = 53.3$. Thus, it is obvious that these harmonic signals may interfere with the detection of $^{50}Cr^+$, $^{52}Cr^+$, $^{53}Cr^+$ and $^{54}Cr^+$ ions and disturb the exploitation of the results. However, the mass resolution obtained with a FTICRMS instrument allows to distinguish chromium isotope ions from harmonic frequencies of lead and lanthanide ions. To evaluate the resonant effect at 357.89 nm, the following ion intensity ratio was calculated:

$$R = \frac{\sum_{i=50}^{54} I_{i\,\mathrm{Cr}^+}}{I_{^{59}\mathrm{Co}^+} + I_{^{120}\mathrm{Sn}^+} + I_{^{142}\mathrm{Nd}^+} + I_{^{152}\mathrm{Sm}^+} + I_{^{153}\mathrm{Eu}^+} + I_{^{155}\mathrm{Gd}^+}}$$

All of the chromium isotopes ($^{50}Cr^+$, $^{52}Cr^+$, $^{53}Cr^+$ and $^{54}Cr^+$) and one isotope for each other doping element (cobalt, tin, neodymium, samarium, europium and gadolinium) were retained. $R = 3.6 \pm 1.1$ and 26.6 ± 2.4 at 355 and 357.89 nm, respectively. The standard deviation was calculated by considering 20 FTICRMS experiments, each experiment being the result of fifty laser shots. The resonant laser ablation/ionization of chromium leads to a significant increase of Cr^+ ion intensity in comparison to other metals. The improvement in signal intensity is, in this case, higher than a factor 7.

The second studied matrix is a polystyrene sample doped with copper and chromium acetylacetonate. Careful optimization was required in the preparation of the sample. At a power density of 4.8×10^8 W/cm^2, the size of the laser spot on the sample was about 130 μm. Consequently, the roughness of the sample had to be as small as possible to limit drift in laser fluence at the sample surface. Smooth films were obtained by using polystyrene (PS). PS was dissolved in tetrahydrofuran and 500 ppm of chromium (i.e., ∼3360 ppm of chromium acetylacetonate) were added. After solvent evaporation, a thin and homogeneous PS film was obtained. To allow comparison between resonant and non-resonant laser ablation, PS was also doped with 500 ppm of copper (i.e., ∼2060 ppm of copper acetylacetonate). The analysis of this sample leads to the observation of the Cr^+ and Cu^+ ions at m/z 50, 52, 53, 54, 63, and 65, respectively. No intense ions of PS matrix were detected. The development of the

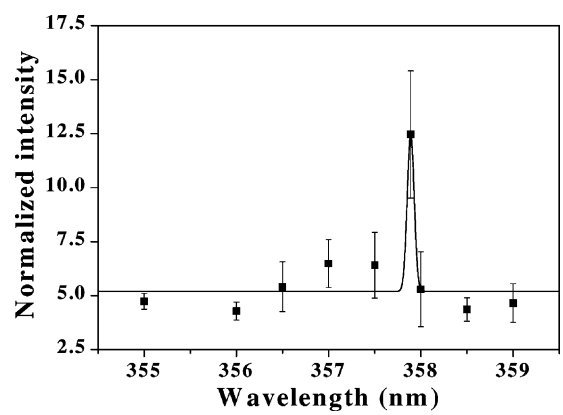

Fig. 7. Development of the chromium in signal in a polystyrene matrix as a function of the wavelength in the neighborhood of 357.87 nm. Normalized intensity is the ratio between the four chromium isotopic signals at m/z 50, 52, 53 and 54 and the two copper ions at m/z 63 and 65.

normalized intensity:

$$\text{Normalized intensity} = \frac{\sum_{i=50}^{54} I_{i\,\mathrm{Cr}^+}}{\sum_{j=63}^{65} I_{j\,\mathrm{Cu}^+}}$$

as a function of the laser ablation wavelength is reported in Fig. 7. It clearly appears a resonance phenomenon at the wavelength of 357.87 nm, with an increase factor of more than 2.5.

4. Discussion and conclusion

The presented results indicate that FTICRMS coupled to RLA constitutes a powerful method in the analysis of inorganic materials. This new technique has indeed, many application fields from elemental analysis (detection of traces in biological, mineral, industrial or geological matrix) to the establishment of relevant methodologies for the speciation as what it was previously established by RLA-ToF-MS [28–30]. If our results are compared to LA-ICP-MS ones, lower detection limits were obtained by LA-FTICR-MS. For example, Guillong and Günther, recently reported a 14 ppm LD for chromium in the study of corundum-based gemstone [38]. Moreover, ICP-MS measurement are often disturbed by isobaric interference which required high mass resolution spectrometers to be resolved [39,40]. This new tool could also be used to improve the understanding of cluster ion formation processes, in particular in the study of mineral compounds by laser ablation [27].

In addition, this study allowed to highlight the influence of power density on the processes which take place in the gas phase after laser ablation/ionization. Similar results obtained by RLA-FTICRMS and LA-FTICRMS at 357.87 and 355 nm, respectively, for irradiances above 5×10^8 W/cm^2 lead us to consider that multiphoton absorption processes require average or low power densities to be efficient. The development of screen effects, when a high power density is used (typically $>10^9$ W/cm^2) limits multiphoton processes due to the important reflectivity of the plume.

Finally, these results may be compared with previous ones obtained by RLA-ToF-MS [23,24]. The results obtained with both techniques are consistent in that, depending on the studied matrix, gain in selectivity by a factor of 2–7 is obtained and the sensitivity is increased. However, it may appear surprising that the selectivity was not significantly improved with RLA-FTICRMS in comparison to RLA-ToF-MS. The reflection geometry of our FTICRMS microprobe [36] should favor multiphoton absorption processes in contrast to the transmission or 45° reflection configuration of the ToF-LMMS instruments [23,24]. The plume expansion in the laser beam direction should improve the efficiency of the resonant processes. Several factors may explain these results. Firstly, there is the photon density distribution when an analysis is carried out with the transmission ToF-LMMS. The power density is maximum at the laser impact, but photons of the laser pulse distribute spatially and temporally into two cones, the node of which is the laser impact. The photons present in the cone located between the impact point and the ToF-MS could to a certain extent (correlation in time and space) lead to resonant processes. Secondly, the wavelengths used in this study are close to the visible field (UV-A), whereas the studies carried out by Verdun et al. [24] used UV-B and UV-C wavelengths. The use of these latter wavelengths limits the thermal aspect of laser/matter interaction and increases photochemical processes. In contrast, for less energetic wavelengths, the thermal effect contribution is more important for the ion formation. Thus, iron [41] and lead oxides [30] differentiation was more efficient when RLA-ToF-LMMS experiments were performed in the UV-C and UV-B wavelength range.

Acknowledgements

The authors gratefully acknowledge a financial support from the Région Lorraine (France).

References

[1] G.S. Hurst, M.G. Payne, S.D. Kramer, J.P. Young, Rev. Mod. Phys. 51 (1979) 767.
[2] G. Rothschopf, J. Zoller, R. Lewis, C. Grant, R. Schur, R. Estler, Int. J. Mass Spectrom. Ion Process. 151 (1995) 167.

[3] K. Wendt, J.V. Kratz, J. Lantzsch, P. Müller, W. Nörtershäuser, A. Seibert, N. Trautmann, A. Waldek, K. Zimmer, Kerntechnik 62 (1997) 81.
[4] R.K. Wunderlich, G.J. Wasserburg, I.D. Hutcheon, G.A. Blake, Anal. Chem. 65 (1993) 1411.
[5] S. Köhler, R. Deissenberger, K. Eberhardt, N. Erdmann, G. Herrmann, G. Huber, J.V. Kratz, M. Nunnemann, G. Passler, P.M. Rao, J. Riegel, N. Trautmann, K. Wendt, Spectrochim. Acta B52 (1997) 717.
[6] L. Johann, R. Stuck, P. Kern, P. Siffert, Analysis 21 (1993) 149.
[7] S.W. Downey, A.B. Emerson, Anal. Chem. 63 (1994) 916.
[8] M. Townie, S.L.T. Drysdale, R. Jennings, A.P. Land, K.W.D. Ledingham, P.T. McCombes, R.P. Singhal, M.H.C. Smyth, C.J. McLean, Int. J. Mass Spectrom. Ion Process. 96 (1990) 309.
[9] G.K. Nicolussi, M.J. Pellin, W.F. Calaway, R.S. Lewis, A.M. Davis, S. Clayton, R.N. Amari, Anal. Chem. 69 (1997) 1140.
[10] H.F. Arlinghaus, N. Thonnard, M.T. Spaar, R.A. Sachleben, F.W. Larimer, R.S. Foote, R.P. Woychik, G.M. Brown, F.V. Sloop, K.B. Jacobson, Anal. Chem. 63 (1991) 402.
[11] J.D. Blum, M.J. Pellin, W.F. Calaway, C.E. Young, D.M. Gruen, I.D. Hutcheon, G.J. Wasserburg, Anal. Chem. 62 (1990) 209.
[12] D.R. Spiegel, W.F. Calaway, A.M. Davis, J.W. Burnett, M.J. Pellin, S.R. Coon, C.E. Young, R.N. Clayton, D.M. Gruen, Anal. Chem. 64 (1992) 469.
[13] D.R. Spiegel, W.F. Calaway, G.A. Curlee, A.M. Davis, R.S. Lewis, M.J. Pellin, D.M. Gruen, R.N. Clayton, Anal. Chem. 66 (1994) 2647.
[14] I.K. Perera, I.C. Lyon, G. Turner, P. Van Lierde, Int. J. Mass Spectrom. Ion Process. 132 (1994) 225.
[15] N.S. Nogar, R.C. Estler, J. Conia, P.J. Jackson, Anal. Chem. 64 (1992) 2972.
[16] S.S. Alimpiev, M.E. Belov, S.M. Nikiforov, Anal. Chem. 65 (1993) 3194.
[17] K. Wendt, K. Blaum, B.A. Bushaw, F. Juston, W. Nörtershäuser, N. Trautmann, B. Wiche, Fresenius J. Anal. Chem. 359 (1997) 361.
[18] B.A. Bushaw, F. Juston, W. Nörthershäuser, N. Trautmann, P. Voss-de Haan, K. Wendt, Resonance ionization spectroscopy, in: N. Winograd, J.E. Parks (Eds.), AIP Conference Proceedings 388, American Institute of Physics, New York, 1996, p. 115.
[19] N. Erdmann, G. Herrmann, G. Huber, S. Köhler, J.V. Kratz, A. Mansel, M. Nunnemann, G. Passler, N. Trautmann, A. Turchin, A. Waldek, Fresenius J. Anal. Chem. 359 (1997) 378.
[20] S.F. Boulyga, N. Erdmann, H. Funk, M.K. Kievets, E.M. Lomonosova, A. Mansel, N. Trautmann, O.I. Yaroshevich, I.V. Zhuk, Radiat. Meas. 28 (1997) 349.
[21] K. Wendt, G. Passler, Phys. Scripta T58 (1995) 104.
[22] M.V. Suryanarayana, M. Sankari, S. Gangadharan, Int. J. Mass Spectrom. Ion Process. 173 (1998) 177.
[23] J.-F. Muller, F. Verdun, G. Krier, M. Lamboulé, S. Gondouin, J.L. Tourmann, D. Muller, S. Lorek, C. R. Acad. Sci. t. 299, Série II 16 (1984) 1113.
[24] F.R. Verdun, G. Krier, J.-F. Muller, Anal. Chem. 59 (1987) 1383.
[25] C. Gill, A.W. Garrett, B.H. Hemberger, S.J. Nogar, J. Am. Soc. Mass Spectrom. 7 (1996) 664.
[26] S. Martinovic, Thesis of the University of Metz, 1997.
[27] A. Hachimi, J.-F. Muller, Chem. Phys. Lett. 268 (1996) 485.
[28] (a) B. Maunit, A. Hachimi, P.J. Calba, G. Krier, J.-F. Muller, Rapid Commun. Mass Spectrom. 9 (1995) 225;
(b) B. Maunit, A. Hachimi, P. Manuelli, P.J. Calba, G. Krier, J.-F. Muller, Int. J. Mass Spectrom. Ion Process. 156 (1996) 173.
[29] A. Hachimi, P. Shirali, G. Krier, J.-F. Muller, J.M. Haguenoer, Toxicol. Environ. Chem. 49 (1995) 13.
[30] N. Chaoui, A. Hachimi, E. Millon, J.-F. Muller, Analysis 24 (1996) 146.
[31] J.K. Gibson, Anal. Chem. 69 (1997) 111.
[32] J.K. Gibson, Radiochim. Acta 81 (1998) 83.
[33] (a) J.-F. Muller, F. Tolitte, G. Krier, M. Pelletier, Brevet Français no. 8809438, 1989;
(b) J.-F. Muller, M. Pelletier, G. Krier, D. Weil, J. Campana, Microbeam analysis, in: P.E. Russell (Ed.), San Francisco Press Inc., San Francisco, 1989, p. 311.
[34] M. Pelletier, G. Krier, J.-F. Muller, D. Weil, M. Johnston, Rapid Commun. Mass Spectrom. 2 (1988) 146.
[35] C.H. Corliss, B.F. Schribner, NBS Monograph (US) 1961, N-32.
[36] J.K. Gibson, Rapid Commun. Mass Spectrom. 10 (1996) 256.
[37] A. Catherinot, B. Angleraud, J. Aubreton, C. Champeaux, C. Germain, C. Girault, Laser processing: Treatment and deposition, in: O. Conde, S. Mazumder, R. Vilar, A. Klumer (Eds.), Academic Publishers, Lisbonne, 1995.
[38] M. Guillong, D. Günther, Spectrochim. Acta Part B 56 (2001) 1219.
[39] K.E. Milgram, F.M. White, K.L. Goodner, C.H. Watson, D.W. Koppenaal, C.J. Baranaga, B.H. Smith, J.D. Winefordner, A.G. Marshall, R.S. Houk, J.R. Eyler, Anal. Chem. 69 (1997) 3714.
[40] C.-H. Wang, C.-J. Chin, S.-K. Luo, L.C. Men, Anal. Chem. Acta 389 (1999) 257.
[41] B. Maunit, Thesis of the University of Metz, 1996.